Available online at www.sciencedirect.com

ScienceDirect

Journal of Crystal Growth 310 (2008) 1627–1631

JOURNAL OF CRYSTAL GROWTH

www.elsevier.com/locate/jcrysgro

Investigation on microstructure in GaN epitaxial growth on the stripe-patterned *r*-plane sapphire substrates

Hou-Guang Chen[a,*], Tsung-Shine Ko[b], Li Chang[c], Yue-Han Wu[c], Tien-Chang Lu[b], Hao-Chung Kuo[b], Shing-Chung Wang[b]

[a]*Department of Materials Science and Engineering, I-Shou University, Kaohsiung 840, Taiwan*
[b]*Department of Photonics & Institute of Electro-Optical Engineering, National Chiao Tung University, Hsinchu 300, Taiwan*
[c]*Department of Materials Science and Engineering, National Chiao Tung University, Hsinchu 300, Taiwan*

Available online 4 December 2007

Abstract

This study reports on the reduction of dislocations in the GaN grown on the stripe-patterned *r*-plane sapphire substrates via metal-organic chemical vapor deposition (MOCVD). The stripes oriented along the sapphire $[1 1 \bar{2} 0]$ direction with asymmetrical side faces were fabricated by lithographic and wet-etching processes. The two etching sides of sapphire-striped mesa are $\{0 0 0 1\}$ and $\{1 \bar{1} 0 1\}$ faces. GaN grown on both etching facets exhibits different epitaxial relationships with the sapphire substrate. The GaN grown from the $\{0 0 0 1\}$ side face of the sapphire mesa contains a low-dislocation density in the order of $10^7\,cm^{-2}$. The interfacial regions between the GaN and patterned sapphire substrate are also studied to clarify the behavior of GaN epitaxial growth on the inclined sapphire faces and defect-reduction mechanism.
© 2007 Elsevier B.V. All rights reserved.

PACS: 68.55.−a; 61.72.Ff; 81.05.Ea; 81.15.Kk; 81.15.Gh

Keywords: A1. Interface; A1. Line defects; A3. Metal-organic vapor-phase epitaxy; B1. Nitrides; B2. Semiconducting III–V materials

1. Introduction

GaN-based heterostructures have been shown to have promising properties for advanced opto-electronic devices, such as light-emitting diodes (LEDs) and laser diodes (LDs). In general, these opto-electronic devices typically consist of an epitaxial multilayer thin-film grown along the [0 0 0 1] direction of the wurtzite crystal structure and encounter the huge built-in electrostatic field that resulted from an intrinsic spontaneous and extrinsic piezoelectric polarization. Hence, the performance of these devices suffers from a strong polarization-induced electric field, which results in reduced overlap between the electron and the hole wave functions in the quantum well [1]. Thus, there has been a considerable interest in the growth of nonpolar or semipolar GaN-based epitaxial film and heterostructures on the *r*-plane sapphire [2], (1 0 0) γ-$LiAlO_2$ [3] and (1 0 0) $MgAlO_2$ [4] substrates to reduce the impact of polarization effect.

Unlike the conventional epitaxial growth of *c*-plane GaN, a nonpolar epilayer grown on the *r*-plane sapphire contains high densities of dislocation and stacking faults due to the large lattice mismatch between GaN and sapphire substrates [2,5]. These extended defects should be eliminated to achieve a high performance of nonpolar GaN devices. Epitaxial lateral overgrown (ELOG) and Pendeo epitaxy (PE) approaches have been demonstrated to be an effective approach for reduction of extended defect density [6,7]. The ELOG and PE process a can dramatically eliminate most of the defects. However, the multiple-step regrowth process is too complicated and time consuming. In addition to ELOG and PE, several groups have proposed that direct lateral epitaxial growth on patterned sapphire substrates (PSSs) can simplify the growth process and enhance device performance and efficiency [8–11].

*Corresponding author. Tel.: +886 7 6577711; fax: +886 7 6578444.
E-mail address: houguang@isu.edu.tw (H.-G. Chen).

0022-0248/$ - see front matter © 2007 Elsevier B.V. All rights reserved.
doi:10.1016/j.jcrysgro.2007.11.178

In our previous work [11], we have demonstrated that GaN grown on patterned *r*-plane sapphire substrates with asymmetrically inclined facets can have a very low-defect density ($10^7\,cm^{-2}$) in GaN epilayers without regrowth process. The present work reports on characterization results of an interfacial microstructure between GaN and PSSs, and presents the possible growth mechanism of GaN on the stripe-patterned *r*-plane sapphire substrates.

2. Experimental procedure

In our study, fabrication of stripe PSSs was illustrated as follows: Plasma-enhanced chemical vapor deposition was used to deposit SiO_2 on *r*-plane sapphire, which was utilized as masks for PSS fabrication. The mask pattern consisted of 1-μm-wide stripes oriented along the $[1\,1\,\bar{2}\,0]$ direction and 6-μm-wide opening as defined by a standard photolithography process. The sapphire substrates were then wet etched using H_3PO_4-based solution at 300 °C for 5 min. Later on, the sample was dipped into a buffered oxide etch (NH_4F:HF = 6:1) solution to remove the SiO_2 mask for the following epitaxial growth. The patterned substrate was loaded into a low-pressure metal-organic chemical vapor deposition (MOCVD) system. An AlN buffer layer was grown at 600 °C, followed by bulk GaN growth at 1120 °C with low V/III ratio of 900–1200 and a pressure of 100 Torr. The microstructure of the GaN on PSS was studied using transmission electron microscopy (TEM). Cross-sectional TEM thin samples were prepared using conventional mechanical polishing and Ar^+ ion milling at 3.5–4 kV. TEM was performed on a Philips Tecnai 20 microscope. Crystallographic analysis and defect characterization for GaN and patterned sapphire were carried out by electron diffraction and bright-field/dark field imaging techniques, respectively.

3. Results and discussion

A low-magnification cross-sectional TEM image of GaN grown on stripe PSS is shown in Fig. 1(a). The GaN is seen to be periodically grown on the stripe PSS. Fig. 1(b) shows the enlarged image of striped mesa, illustrating that the inclined angles of two side faces of sapphire mesa are different. Hence, it suggests that the two side etching facets are terminated by different crystallographic faces. According to diffraction patterns, both side faces of sapphire-striped mesa are near $\{0\,0\,0\,1\}$ and $\{1\,\bar{1}\,0\,1\}$, respectively, deviated from nominal faces by several degrees. The low symmetry of the *r*-face sapphire along $[1\,1\,\bar{2}\,0]$ causes the emergence of asymmetrically etched faces between both sides of the mesa. Each GaN grown on the striped mesa can be considered as consisting of two crystallites (designated as GaN I and GaN II) terminated with various facets, as shown in Fig. 1(c). It is remarkable to see GaN I grown on the top face and right-side face of the sapphire-striped mesa, and the GaN II grown on the left-side face region. To realize the

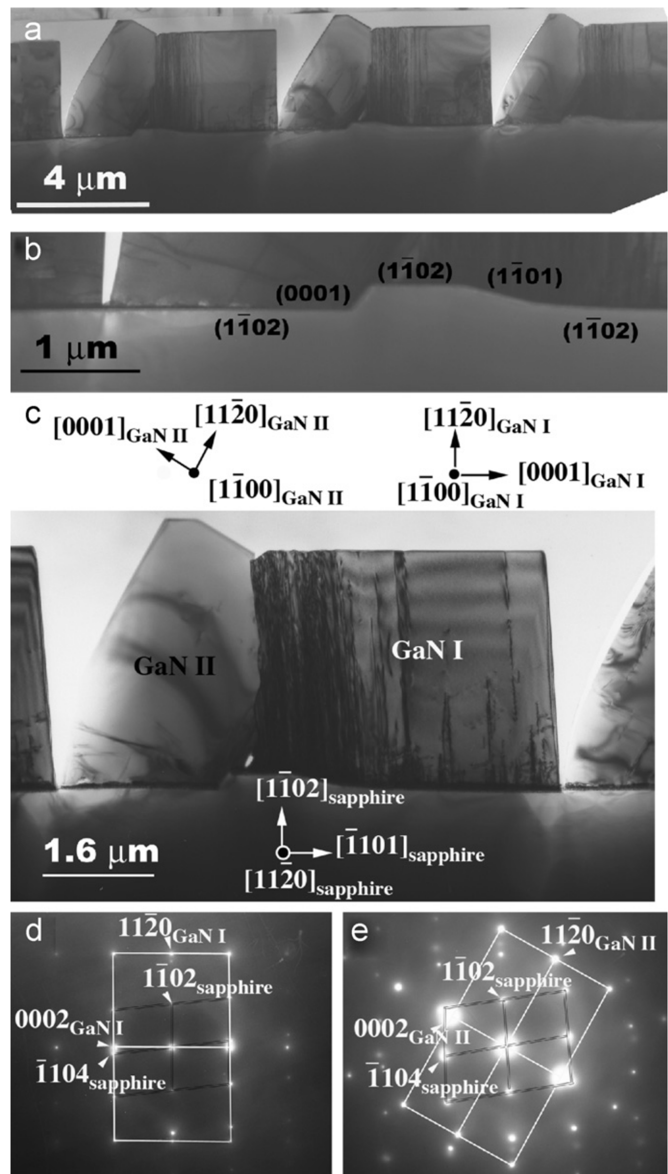

Fig. 1. (a) Bright-field TEM image of GaN grown on stripe-patterned sapphire substrate. (b) Enlarged image of side etching faces of sapphire striped mesa. (c) Bright-field image of one complete GaN stripe and schematic representation of orientation relationship among GaN I, GaN II, and sapphire substrate. (d) and (e) SAD patterns taken from the interface region between sapphire and GaN I and between sapphire GaN II.

crystallographic relationships among GaN I, GaN II, and sapphire substrate, selected area diffraction (SAD) patterns were taken from interfacial regions between GaN I and sapphire substrate, and GaN II and sapphire substrate, respectively (Fig. 1(d) and (e)). Based on the diffraction patterns, the crystallographic relationship between GaN I and sapphire is established as $(1\,1\,\bar{2}\,0)_{GaN} \| (1\,\bar{1}\,0\,2)_{sapphire}$ and $[1\,\bar{1}\,0\,0]_{GaN} \| [1\,1\,\bar{2}\,0]_{sapphire}$. However, the crystallographic relationship between GaN II and sapphire substrate is shown to be $(0\,0\,0\,1)_{GaN} \| (0\,0\,0\,1)_{sapphire}$ and $[1\,\bar{1}\,0\,0]_{GaN} \| [1\,1\,\bar{2}\,0]_{sapphire}$. The schematic representation of orientation relationships among GaN I, GaN II, and

sapphire substrate is drawn in Fig. 1(c). The top and lateral faces of GaN I are $(1 1 \bar{2} 0)$ and $(0 0 0 1)$ faces, respectively. The orientation relationship between GaN I and sapphire substrate is usually seen in the case of a GaN epitaxially grown on an *r*-plane sapphire. In the GaN II, however, the top face GaN II parallel to the *r*-plane sapphire is semipolar face $(1 1 \bar{2} 2)$, while inclined faces of GaN II on the right and left sides are $(1 1 \bar{2} 0)$ and $(0 0 0 1)$ faces, respectively. The growth of GaN II originating from the $(0 0 0 1)$ side face of sapphire-striped mesa results in another epitaxial relationship of GaN on a sapphire substrate.

The distributions of defect density in GaN vary in different regions (Fig. 1(c)). Detailed analysis of the defect densities from the top-view SEM and two-beam dark-field TEM images has been shown elsewhere [11]. In the GaN I, a high-defect density ($>10^{10}\,cm^{-2}$) exists in the region above the top face and right-side faces of the mesa. These defects include threading dislocations (TDs) and stacking faults (SFs) that are often found in *a*-plane GaN epitaxially grown on the *r*-plane sapphire substrate. However, the dislocation density reduces to $4 \times 10^{8}\,cm^{-2}$ in the lateral region. In contrast, the defect density is dramatically eliminated ($10^{7}\,cm^{-2}$) in GaN II. It is possible that lateral epitaxial growth of GaN leads to the reduction of defect density. In particular, the low-defect density regions of GaN grow on both lateral regions of the mesa. The development of the lateral growth of GaN will be discussed in the following:

As mentioned above, the GaN II might grow directly from the $\{0 0 0 1\}$ side face of sapphire mesa. To investigate the lateral growth of GaN II from the $\{0 0 0 1\}$ sapphire side face, the interface between GaN II and the $\{0 0 0 1\}$ side face and neighbored *r*-plane sapphire face were examined in TEM. According to the growth procedure, prior to GaN growth, a low-temperature AlN nucleation layer was deposited on PSS. From the high-magnification TEM image in Fig. 2(a), the AlN nucleation layer with uniform thickness (5 nm) is covered on the $\{0 0 0 1\}$ side face and neighbor *r*-plane surface. The insets show two SAD patterns in the sapphire $[1 1 \bar{2} 0]$ zone axis taken from the interface regions on the {0001} side face and on the sapphire *r*-plane region, respectively. Notably, the crystallographic orientation of AlN grown on the $\{0 0 0 1\}$ side face (designated as *c*-AlN) differs from the AlN grown on neighbor *r*-plane faces (designated as *a*-AlN). The epitaxial orientation relationship of AlN layer grown on the $\{0 0 0 1\}$ side face of mesa is $(0 0 0 1)_{AlN} \| (0 0 0 1)_{sapphire}$ and $[1 \bar{1} 0 0]_{AlN} \| [1 1 \bar{2} 0]_{sapphire}$, which is the same as in the case of GaN II, as shown in the bottom-right inset, while the up-left inset shows that the orientation relationship of AlN grown on the neighbor *r*-plane sapphire region is $(1 1 \bar{2} 0)_{AlN} \| (1 \bar{1} 0 2)_{sapphire}$ and $[1 \bar{1} 0 0]_{AlN} \| [1 1 \bar{2} 0]_{sapphire}$. Figs. 2(b) and (c) show the dark-field images of AlN grown on $\{0 0 0 1\}$side face and neighbor *r*-plane sapphire faces, respectively, which give direct evidence for the variation of crystallographic orientation of the AlN layer grown on different sapphire faces. According to the SAD results and dark-field images of the AlN nucleation layer, the growth of GaN II should originate from the $\{0 0 0 1\}$ side face of mesa, because the crystallographic orientation of GaN II is consistent with that of *c*-AlN. In addition, we have also found several island-shaped crystallites with dark contrast at the interface between GaN II and *a*-AlN, as shown in Fig. 3(a). Based on the sapphire $[1 1 \bar{2} 0]$ zone axis SAD analysis (Fig. 3(b)), the dark islands are indeed GaN (designated as GaN III) with the same crystallographic orientation as the underlying *a*-AlN instead of GaN II. It is evident that GaN can also directly grow on the *a*-AlN in the initial growth stage. Fig. 3(c) is a dark-field image of

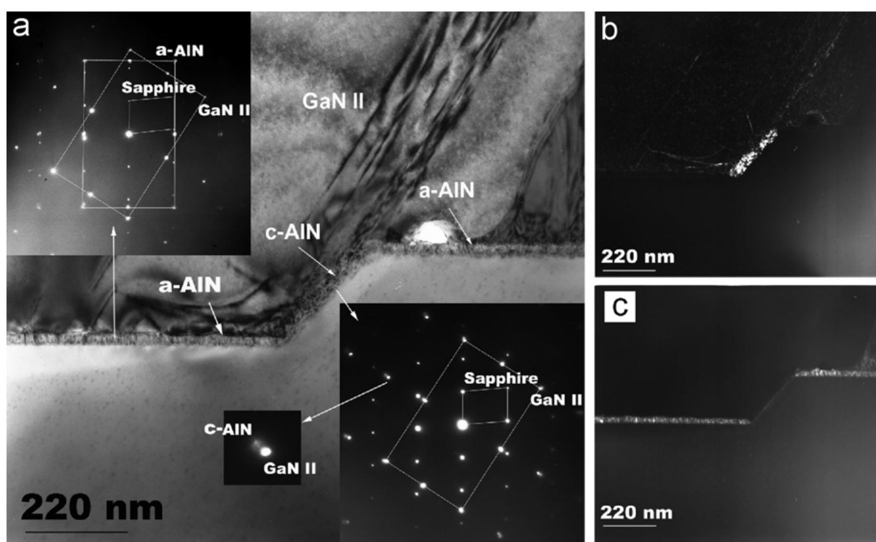

Fig. 2. (a) TEM image of interface between GaN II and the $\{0 0 0 1\}$ side face of sapphire mesa and neighbor *r*-plane sapphire face. Insets showing the SAD patterns in sapphire $[1 1 \bar{2} 0]$ zone axis corresponding to the two regions, as indicated by white arrows. (b) and (c) Dark-field images of AlN grown on $\{0 0 0 1\}$ side face of sapphire mesa (*c*-AlN) and AlN grown on neighbor *r*-plane sapphire face (*a*-AlN).

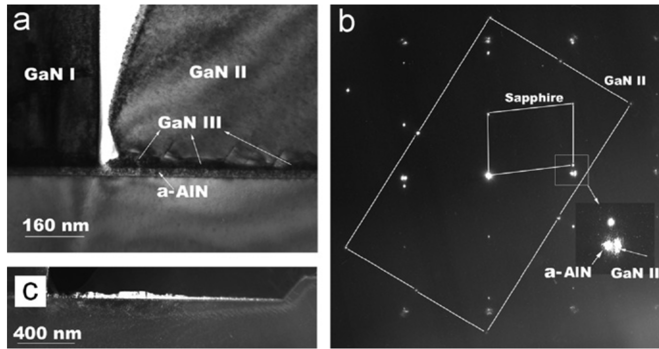

Fig. 3. (a) Island-shaped crystallites grown at the interface between GaN II and *a*-AlN. (b) SAD pattern of the island-shaped crystallites in sapphire $[1 1 \bar{2} 0]$ zone axis. (c) Dark-field image showing the distribution of island-shaped crystallites (GaN III) grown on *a*-AlN.

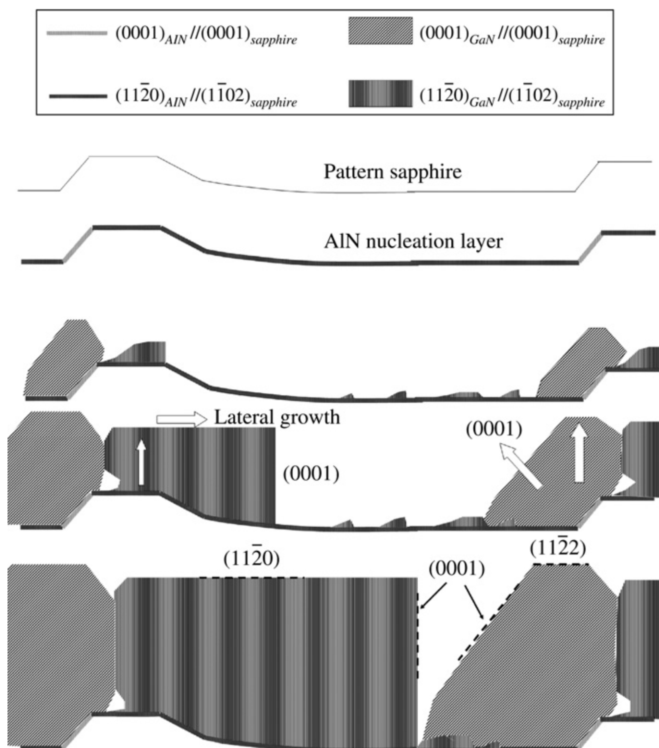

Fig. 4. Schematic representation of the evolution of GaN growth on the patterned sapphire.

GaN III directly grown on *a*-AlN. It is observed that the height of the GaN III increases with the distance away from the mesa. According to TEM, we can deduce that the overgrown GaN II prevents GaN III on *a*-AlN from further growth in the following growth stage. Therefore, the overall growth rate of GaN grown from the $\{0 0 0 1\}$ side face of sapphire mesa must be higher than that of GaN directly grown on AlN deposited on the *r*-plane sapphire face. In general condition for the growth of nonpolar *a*-plane GaN, the growth rate along $\{0 0 0 1\}$ growth fronts is higher than that on $\{1 1 \bar{2} 0\}$ face and other faces, resulting in a stripe feature on the $(1 1 \bar{2} 0)$ GaN epilayer surface [12]. In addition, recently, Ni et al. [13] have reported epitaxial lateral overgrowth of $(1 1 \bar{2} 2)$ semipolar GaN grown on *m*-plane sapphire substrates. According to their results, GaN with a low-defect density ($10^7\,cm^{-2}$) also can be obtained from the inclined wing grown along the $[0 0 0 1]$ direction. The growth along the $[0 0 0 1]$ axis advances faster than those in other directions. Their results are very similar to our case.

In summary, the evolution of GaN growth on the pattern sapphire can be schematically illustrated in Fig. 4. In the first stage, the AlN nucleation layer can cover all over the surface of the PSS. The crystallographic orientations of the AlN layer grown on the $\{0 0 0 1\}$ side face of mesa is in *c*-plane different from *a*-AlN grown on other regions. Then, GaN nucleates on the AlN layer, but the GaN nuclei on the $\{0 0 0 1\}$ side faces and the top face of mesa may have higher growth rate along the *c*-axis direction than those on other regions. In the following growth stage, the GaN lateral overgrowth from the top and the $\{0 0 0 1\}$ side faces of the mesa will occur. Later on, the overgrowth of GaN I results in coalescence with the GaN islands that originally nucleate on the *a*-AlN layer due to the consistent crystallographic orientations between them, and at the same time the GaN II grown from the $\{0 0 0 1\}$ side faces of the mesa will overgrow the GaN islands and prevent these GaN islands from further growth. Finally, the growth fronts of GaN I and GaN II will meet.

4. Conclusion

In this study, we show that GaN grown on an *r*-plane stripe PSSs has a low-defect density. On both side-etched facets of the striped mesa sapphire substrates, two GaN crystallites are epitaxially grown in different orientations, which are $(1 1 \bar{2} 0)_{GaN} \| (1 \bar{1} 0 2)_{sapphire}$ and $[1 \bar{1} 0 0]_{GaN} \| [1 1 \bar{2} 0]_{sapphire}$, and $(0 0 0 1)_{GaN} \| (0 0 0 1)_{sapphire}$ and $[1 \bar{1} 0 0]_{GaN} \| [1 1 \bar{2} 0]_{sapphire}$, respectively. The GaN grown on the $(0 0 0 1)$ side face of the sapphire mesa contains a low-dislocation density in the order of $10^7\,cm^{-2}$. Characterization of interfacial microstructures on various regions shows that the AlN nucleation layer has the same characteristics as GaN, and the development of GaN through the lateral epitaxial growth mechanism along the *c*-axis is established.

Acknowledgments

This work was supported by the National Science Council of the Republic of China (ROC) under Contract nos. NSC 95-2120-M-009-008, NSC 95-2218-E-214-003, and NSC 96-2221-E-214-027.

References

[1] P. Waltereit, O. Brandt, A. Trampert, H.T. Grahn, J. Menniger, M. Ramsteiner, M. Reiche, K.H. Ploog, Nature 406 (2000) 865.

[2] M.D. Craven, S.H. Lim, F. Wu, J.S. Speck, S.P. DenBaars, Appl. Phys. Lett. 81 (2002) 469.

[3] P. Waltereit, O. Brandt, M. Ramsteiner, A. Trampert, H.T. Grahn, J. Menniger, M. Reiche, K.H. Ploog, J. Crystal Growth 227–228 (2001) 437.

[4] J.F. Kaeding, M. Iza, H. Sato, S.P. DenBaars, J.S. Speck, S. Nakamura, Jpn. J. Appl. Phys. 45 (2006) L536.

[5] X. Ni, Y. Fu, Y.T. Moon, N. Biyikli, H. Morkoc, J. Crystal Growth 290 (2006) 166.

[6] W. Zhou, D. Ren, P.D. Dapkus, J. Crystal Growth 290 (2006) 11.

[7] T.C. Wang, T.C. Lu, T.S. Ko, H.C. Kuo, M. Yu, S.C. Wang, C.C. Chou, Z.H. Lee, H.G. Chen, Appl. Phys. Lett. 89 (2006) 251109.

[8] Y.J. Lee, J.M. Hwang, T.C. Hsu, M.H. Hsieh, M.J. Jou, B.J. Lee, T.C. Lu, H.C. Kuo, S.C. Wang, IEEE Photon. Technol. Lett. 18 (2006) 1152.

[9] D.S. Wuu, W.K. Wang, K.S. Wen, S.C. Huang, S.H. Lin, S.Y. Huang, C.F. Lin, R.H. Horng, Appl. Phys. Lett. 89 (2006) 161105.

[10] T.S. Ko, T.C. Wang, R.C. Gao, Y.J. Lee, T.C. Lu, H.C. Kuo, S.C. Wang, H.G. Chen, Appl. Phys. Lett. 90 (2007) 013110.

[11] H.G. Chen, T.S. Ko, S.C. Ling, T.C. Lu, H.C. Kuo, S.C. Wang, Y.H. Wu, L. Chang, Appl. Phys. Lett. 91 (2007) 021914.

[12] H. Wang, C. Chen, Z. Gong, J. Zhang, M. Gaevski, M. Su, J. Yang, M.A. Khan, Appl. Phys. Lett. 84 (2004) 499.

[13] X. Ni, U. Ozgur, A.A. Baski, H. Morkoc, L. Zhou, D.J. Smith, C.A. Tran, Appl. Phys. Lett. 90 (2007) 182109.